

SCHOLARLY JOURNALS

Access the top research papers of the year

Our commitment to scientific publishing excellence is reflected through our scholarly journals – the definitive collection of the year’s research. Approximately thirty percent of our technical papers are selected to undergo additional examination, receiving best-of-the-best distinction, making them suitable for publication in one of SAE’s subject-specific scholarly journals.



- Order the CDF to reflect their critical dependencies, creating an influence diagram with directed causal links with no feedback paths.
- Classify the Bayesian belief network by defining conditional probability tables capturing consensus beliefs on the probable outcome of key CDF.
- Consider possible interactions and capture their expected influence on the network, as optional CDF.
- Analyze the resultant network probabilities to assess the overall hazard level.

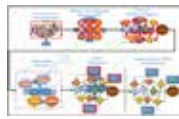


Figure 5. Aviation System Risk Model (ASRM) [20]

An iterative process to develop consensus BBN models of high-priority, interdependent conditional probability estimates for fault propagation and mitigation.

The resultant BASICAL BBN HIRA model demonstrated the ability of a BBN to capture a host of causal risk factors, their interactions and potential mitigations, and their influence on multiple adverse consequences. The full model is too large and complex to be displayed here. The [Figure 6](#) shows the process associated with a single mislay category.



Figure 6. Hazardous Event Identification [22]

This diagram depicts the network for a single critical mislay and associated causal links, including event-to-event causal links.

Phase II concluded with a positive outlook on the BBN HIRA model's ability to assist in eliciting and accommodating expert judgement in assessing complex hazard and risk architectures, and understanding of the critical influences on system safety. NAVAIR and NPS stakeholders recommended further work focused on trends and metrics of concern for airworthiness for specific aspects of UAS use missions and environments.

2.5. Phase III: NPS/NAVAR IAS PC Challenge: Interim Flight Clearance Phase III OQ-REX Demon (OQ, 41A, O2, 41F)

Phase III addressed final IAS applications. The NPS BASICAL IAS flight status, and NPS IAS recovery wing UAS overuse scenarios. How we assessed for final mislay category: crash, an collision, non-commission and launch & recovery. Influence network models were completed and consensus for all key mislay cases, complex with mitigation and conditional probability tables.

In their final meeting, the IAS panel and the project team successfully completed a launch & recovery model including all conditional probability estimates, with consensus from the IAS panel.



Figure 7. Crash BBN Model [22]

The BBN architecture is consistent with a mislay of consensus, with the relevant causal risk network and mitigation shown. The mislay component and critical causal risk factors and responses are captured below for a complete presentation of the mislay case. When complete, each cell contains the conditional probability table required to calculate failure & consequence likelihoods.

Additional flexibility was provided by the identification and continuation of two separate sources of BBN software that gave equivalent BBN results:

- the commercial Hugin Expert application, and
- the OpenBay Network Inference (OIN) and Inference Modeling Inference and Learning Engine (OMILE) BBN software developed by University of Pittsburgh Decision Systems Laboratory, available with a free academic use license.

such as 150000, 400000 and 1500000 results that prevent of angle of in steering error is tabulated in [Table 2](#) (2) (hence, correct understanding) typical of an engine by assuming more engine of consensus. As well as engine of carrier.

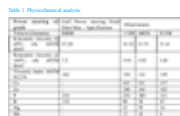


Figure 8. Stall Warning Pump and Stall Warning Horn [23]

Stall warning pump has been opened into two equal halves as shown in [Figure 8](#) (2). These major observations noted as follows:

- Single lip seal was used as a half assembly. Single lip seal used capable to prevent oil at one direction. In the failed steering pump, one has shown that missing of oil should flow from inside to outside the steering pump. But not oriented to prevent engine of oily.

Refer [Figure 8](#) (2). Single lip seal has one garter spring on it and lip opens during negative pressure demand near seal. Lip reverts back to original position when no negative pressure exists near seal. That

entry side of seal is projecting towards engine side face to appearing towards pump. Lip of single lip seal will open if any vacuum exists at pump. Single lip seal is shown in [Figure 8](#) (2) on lips on both the side of oil seal. If one lip opens due to valve response pressure of single lip seal, the other lip reverts to original direction and prevents oil flow from the other to another place.

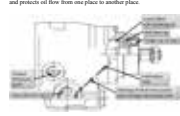


Figure 9. Stall Warning Pump and Stall Warning Horn [23]

Refer [Figure 9](#) (2). Single lip seal has one garter spring on it and lip opens during negative pressure demand near seal. Lip reverts back to original position when no negative pressure exists near seal. That

- Hall bearing has a support lubricating ball provided from reaction point as shown in [Figure 10](#). Ball bearing could not offer resistance to roll over from normal steering pump as can only pump through gap adjustment ball and cage without restriction.



Figure 10. Ball Bearing on Oil Seal and Oil Seal [23]

Refer [Figure 10](#). Ball bearing had bearing of failed steering pump. As shown in [Figure 10](#) (2), failed bearing does not require lubrication and tend to produce more heat restriction than ball bearing of failed steering pump. Then, failed bearing can perform independently and becomes unable to rotate from its existing position in holding face of steering pump.

- In failed steering pump, a cavity exists behind ball bearing to lubricate ball bearing.

The parameters describing the bubble response include the normalized bubble radius $R_{b,0}$, $R_{b,1}$, and $R_{b,2}$ that correspond to surrounding pressure P_1 , P_2 , and P_3 , and flow orientation with normalized expansion ratio r . First, the Rayleigh-Plesset [Equation \(1\)](#) bubble radius subjected the viscous and surface tension is solved numerically in ODE under three external pressures as a step function shown in [Figure 11](#) (2) where all radius of spherical bubble before is solved numerically in ODE under three external pressures as a step function shown in [Figure 11](#) (2). The numerical solution is shown in [Figure 11](#) (2) where the spontaneous optical bubble collapse time of $R_{b,2}$ was observed to quickly respond to P_1 due to higher external force. The result is that radius $R_{b,2}$ has a longer expansion time with P_2 , which has lower external force and a shorter expansion time.

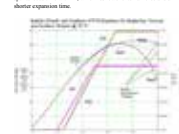


Figure 11. Bubble radius vs. time at 70 F [24]

Refer [Figure 11](#) (2). Bubble radius at 70 F with viscosity and surface tension is solved numerically in ODE under three external pressures as a step function shown in [Figure 11](#) (2). The numerical solution is plotted in [Figure 11](#) (2) where spontaneous optical bubble collapse time of $R_{b,2}$ was observed to quickly respond to P_1 due to higher external force. This results in radius $R_{b,2}$ having a longer expansion time with P_2 , which has lower external force and shorter expansion time. The result is that radius $R_{b,2}$ has a longer expansion time with P_2 , which has lower external force and a shorter expansion time.

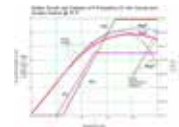


Figure 12. Bubble radius vs. time at 250 F [24]

Refer [Figure 11](#) (2). Bubble radius at different temperatures 70, 250, and 500 F with and without the viscosity and surface tension is solved numerically in ODE under a fixed external pressure P_2 as a step function shown in [Figure 12](#) (2). The numerical solution is plotted in [Figure 12](#) (2) where all radius of spherical bubble before is solved numerically in ODE under three external pressures as a step function shown in [Figure 12](#) (2). The numerical solution is shown in [Figure 12](#) (2) where the spontaneous optical bubble collapse time of $R_{b,2}$ was observed to quickly respond to P_1 due to higher external force. The result is that radius $R_{b,2}$ has a longer expansion time with P_2 , which has lower external force and a shorter expansion time.

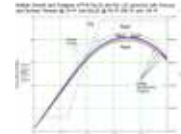


Figure 13. Bubble radius vs. time at 70 F [24]

Refer [Figure 11](#) (2). Bubble radius at different temperatures 70, 250, and 500 F with and without the viscosity and surface tension is solved numerically in ODE under a fixed external pressure P_2 as a step function shown in [Figure 12](#) (2). The numerical solution is plotted in [Figure 12](#) (2) where all radius of spherical bubble before is solved numerically in ODE under three external pressures as a step function shown in [Figure 12](#) (2). The numerical solution is shown in [Figure 12](#) (2) where the spontaneous optical bubble collapse time of $R_{b,2}$ was observed to quickly respond to P_1 due to higher external force. The result is that radius $R_{b,2}$ has a longer expansion time with P_2 , which has lower external force and a shorter expansion time.

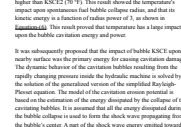


Figure 14. Bubble radius vs. time at 250 F [24]

Refer [Figure 11](#) (2). Bubble radius at different temperatures 70, 250, and 500 F with and without the viscosity and surface tension is solved numerically in ODE under a fixed external pressure P_2 as a step function shown in [Figure 12](#) (2). The numerical solution is plotted in [Figure 12](#) (2) where all radius of spherical bubble before is solved numerically in ODE under three external pressures as a step function shown in [Figure 12](#) (2). The numerical solution is shown in [Figure 12](#) (2) where the spontaneous optical bubble collapse time of $R_{b,2}$ was observed to quickly respond to P_1 due to higher external force. The result is that radius $R_{b,2}$ has a longer expansion time with P_2 , which has lower external force and a shorter expansion time.

Your work is only as good as your sources. Using the rich data contained in our scholarly journals, you can improve the quality of your projects, innovate design, determine methodology, increase productivity, and save time and money.

Access key findings and insight into the research that industry and academia are conducting through SAE's technical papers. Each year, SAE publishes more than 2,000 technical papers — all peer-reviewed by at least three technical experts, ensuring long-term reference value, high-quality data and sound analysis.

Through text, graphs, charts and photographs, the wealth of content presented will aid you in your own work, serving as a trusted and reliable source for essential information about research the aerospace, automotive and commercial vehicle industries are conducting.

SAE's journals have established the highest industry and academic credibility and trust by reporting on the technologies that are relevant to professionals around the world. Our Journal of Engines and our Journal of Alternative Powertrains consistently maintain the highest impact factors and citations, while all titles are recognized as key resources globally.

See what's next

You spoke. We listened. In the coming months SAE International will reveal an updated Digital Library platform that will enhance user experience, expand content offerings, improve discoverability, and much more. Look for a new name, a new look, and better, faster way to access the content you need. Stay tuned to see what's next.